Lasers in Manufacturing Conference 2023

In-situ detection of defect formation during Laser Metal Deposition by melt pool monitoring using coaxial CCD-camera

Johannes Käsbauer[a,*], Korbinian Schröcker[a], David Scheider[b], Martin Reisacher[b], Andrey Prihodovsky[a]

[a]Technische Hochschule Deggendorf, Technologie Campus Parsberg-Lupburg, Am Campus 1, 92331 Parsberg, Germany
[b]DMG MORI Ultrasonic Lasertec GmbH, DECKEL MAHO-Straße 1, 87459 Pfronten, Germany

Abstract

Powder-based Laser Metal Deposition offers great opportunities for the manufacturing of components for various applications. To ensure the high load-bearing capacity of these technical parts, the formation of internal defects must be avoided. Thus, appropriate process properties need to be maintained during the entire manufacturing sequence by using suitable processing parameters. In this work, samples are built out of the material Ferro 55. During the building process, the melt pool characteristics are monitored using a CCD camera, whose optical path is coaxial to the processing laser beam. By investigating the obtained images, the melt pool size is selected as a value that allows for the assessment of the deposition process. The correlation of the temporal progression of the melt pool size with metallographic investigations of the samples shows that the formation of lack of fusion defects can be detected as the melt pool size descends below a specific threshold.

Keywords: Laser Metal Deposition; Additive Manufacturing; process monitoring; defect formation; Ferro 55

1. Introduction

DED processes like laser metal deposition (LMD) are used for the manufacturing and repair processes of components for various applications (Bennett et al. 2019; Dey; Perini 2020; Bohlen et al. 2018). In the process, a metal surface is locally irradiated by a moving laser beam so that a pool of molten material is formed. Additional metallic powder is brought into the melt pool so that the powder is melted. Further movement of

* Corresponding author. Tel.: +49-9492-8384-107.
E-mail address: johannes.kaesbauer@th-deg.de.

the laser beam leads to the local cooling and solidification of the molten material, which cools down so that a weld bead is formed. Several parallel and overlapping weld beads usually build a planar layer of deposited material. By depositing further layers on top, three-dimensional structures are formed.

Using LMD, many different materials can be processed. By applying appropriate process properties, structures with high strength and hardness and low porosity are possible. To obtain appropriate process properties, the process parameters often need to be adjusted during the build-up of the components as local temperatures vary (Schröcker et al. 2022). During inappropriate processing conditions, the occurrence of cracks, lack of fusion defects and gas pores may increase (Dass und Moridi 2019).

For quality assurance, various methods of analysis are used. Hereto, non-destructive methods such as X-ray and ultrasonic scans as well as destructive methods like the metallographic analysis of cross sections are to be mentioned (Benarji et al. 2020; Dass et al. 2022; Kersten et al. 2020; Schröcker et al. 2022; Rey et al. 2022; Thompson et al. 2016).

In favor of cost reduction, it is aspired to prevent the formation of defects during the LMD process. Therefore, various monitoring methods are developed. In (Dass et al. 2022; Wolff et al. 2021) X-ray tomography is used for monitoring keyhole and pore formation. Other developments follow the approach of monitoring the process on the part's surface. For this purpose, the melt pool is monitored using cameras (Ocylok et al. 2014; Kledwig et al. 2019; Turichin et al. 2022; Khanzadeh et al. 2019). Thus, the influence of various process parameters on the melt pool characteristics is observable. Based on the camera signals, a number of approaches for controlling process parameters have been developed (Liu et al. 2019; Smoqi et al. 2022).

The aim of this work is to investigate the potential of the camera-based melt pool monitoring system described by (Kledwig et al. 2019), for the detection of defect formation during the build-up of components by LMD. Especially the influence of the manufacturing sequence on the gathered monitoring data is investigated.

2. Material and methods

In order to investigate the manufacturing process, samples are built up while the melt pool characteristics are monitored. Subsequently, the samples are prepared for post-process analysis.

2.1. Build-up process and equipment

For the experimental investigations, a Lasertec 65 DED hybrid machine by the manufacturer DMG MORI Ultrasonic Lasertec GmbH is used. The machine and its nozzle are shown in Fig. 1.

Fig. 1. DMG MORI Lasertec 65 DED hybrid (left); LMD coaxial nozzle (right)

It is equipped with a coaxial powder nozzle and a diode laser, generating a laser spot with a 3 mm diameter on the workpiece. The laser's wavelength is 1020 nm.

Mild steel plates (material: S235JR, 350 mm x 100 mm x 10 mm) are used as a substrate. Before material deposition, the substrate plates are cleaned with ethanol. Commercially available gas-atomized Ferro 55 powder is used. According to the material supplier datasheet (voestalpine Böhler Welding Group GmbH), the nominal chemical composition is 0.35 wt.% C, 7.0 wt.% Cr, 2.2 wt.% Mo, 1.1 wt.% Mn, 0.3 wt.% Si, Fe balance.

The specimens are made of multiple square shaped layers. One sample block made of 32 layers is shown in Fig. 2 on the right. The trajectory of one layer is shown in Fig. 2 on the left. At first, the infill deposition is carried out in a zigzag manner (see red arrows in Fig. 2). During the motion between each infill line, the laser is switched off shortly (blue lines in Fig. 2). After the layer's infill paths are finished, the contour lines are carried out (violet lines in Fig. 2). The offset between adjacent infill paths is 1.4 mm. The distance between contour and infill paths is 1 mm. After one layer is finished, the next layer is placed on top with a vertical offset of 0.89 mm. Each layer is manufactured using the same pattern of trajectories. Though the trajectories are rotated by 90° in respect to those of the previous layer.

During the build-up of a sample, heat accumulation takes place. Furthermore, the heat conduction conditions from the melt pool change, as the distance to the substrate plate increases from layer to layer. Due to the heat accumulation, it is to be expected, that the laser power needs to be reduced to a certain value, to prevent the part from overheating. Therefore, an initial laser power of 2 kW, selected for the first layer, is gradually reduced by 100 W per layer until a value of 1 kW is reached in the eleventh layer. For all following layers, 1 kW is kept. The powder mass flow is set to 12 g/min for the entire build-up process. The nozzle's travel speed during infill and contour paths is 1 m/min.
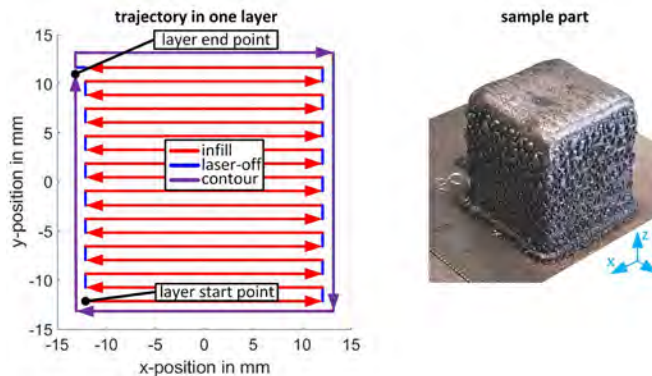
Fig. 2. Laser spot trajectory in every layer (left); LMD-manufactured sample (right).

2.2. Process monitoring and defect detection

In order to monitor the process sequence, a CCD camera is used. The operation principle of the monitoring system is shown in Fig. 3. Using a dichroic mirror, the camera's optical path is coaxial to the processing laser beam (see Fig. 3). This way, the heat radiation emitted from the melt pool is monitored, regardless of the nozzle's position relative to the workpiece. The wavelength observed by the camera is limited to 740 nm by a filter. The optical setup used for process monitoring in this work is described in (Kledwig et al. 2019) in more detail.

The camera yields images of the melt pool and the adjacent area, showing the locally detected intensity of heat radiation. The camera is calibrated in order to link the detected intensity to the local temperature (Kledwig et al. 2019). For detailed monitoring of the temporal process sequence, a relatively high sample rate

of 20 Hz is used in this work. As described in (Kledwig et al. 2019), only the circular region of interest is extracted from the camera images. An exemplary figure obtained during the process is shown in Fig. 3.

A metric defining the melt pool area must be extracted from each figure in order to characterize the temporal evolution of the melt pool. The figures are subsequently binarized based on the brightness of each pixel. The intensity at the material's melting point is chosen as the threshold value. All points with intensities greater than the threshold are taken to represent molten material. In this manner, each camera frame's pixels are identified as either being inside the melt pool or not. An example of a binarized camera image is provided in Fig. 3 on the right. The number of pixels assigned to the melt pool is a statistic that is sensitive to the process parameters in LMD, as stated in (Kledwig et al., 2019). This work also uses the metric known as the monitored melt pool size.
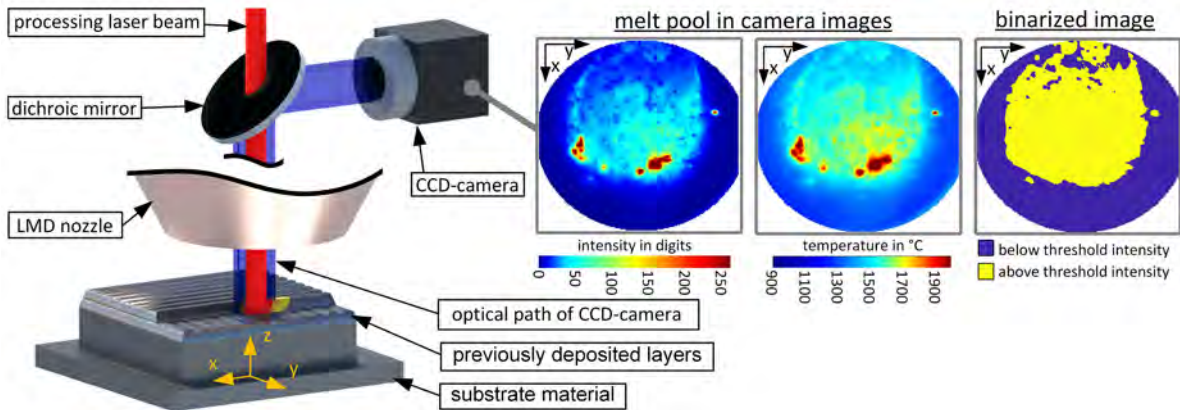
Fig. 3. Optical paths of laser beam and camera (left); exemplary camera images of the melt pool (right).

Fig. 4 shows an example of the temporal course of the monitored melt pool size. The shown signal is gathered within the manufacturing of the first six layers of the sample block depicted in Fig. 2. In the signal, several peaks are visible. Moreover, the signal frequently drops to zero. The mean size seems to decrease with time.
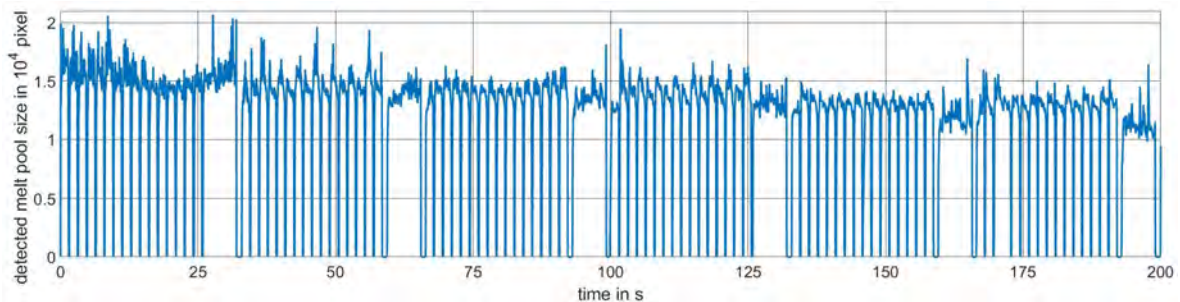
Fig. 4. Exemplary temporal progression of detected melt pool size.

To draw conclusions on the melt pool characteristics, the temporal progression of the process signal needs to be investigated. Especially the causes for intense fluctuations in the data and their appropriate handling need to be analysed. To ease the monitoring of process characteristics and the control of process parameters, criteria for the assessment of the signals need to be determined. For this reason, the monitoring data must be examined with simultaneous consideration of the detected internal defects in the manufactured part. These

internal defects can be observed after the build-up blocks are cut in half, the cutting surfaces are polished, etched and investigated using optical microscopy.

3. Analysis of monitored process characteristics

3.1. Categorization of data according to manufacturing sequence

As the manufacturing sequence contains infill, contour and laser-off trajectories (Fig. 2), the interaction between laser, powder and the part's surface changes throughout the entire process. This is schematically illustrated by Fig. 5, showing an infill and a contour path in a top view perspective. Following an infill path, the laser energy from the entire spot area hits the surface that the current layer is being built on. On the contrary, during contour paths, the cross-section of the laser beam and the part's surface do not overlap completely. Consequently, only a fraction of the emitted laser radiation reaches the layer surface in contour paths. Therefore, it is expected that during contour paths, less laser energy is transferred compared to infill paths. The powder catchment efficiency can vary between infill and contour paths as well.

Furthermore, thermal conditions for the heat dissipation from the laser spot on the part surface into the bulk material at contour paths differ significantly from those at infill paths. Local thermal conditions within an infill path are also not constant and differ significantly near part edges – that means at the start and the end – from those in the middle of a path.

The amount of laser radiation and powder brought to the part's surface and the local thermal conditions have a decisive impact on the melt pool characteristics. Therefore, processing conditions need to be considered when examining the collected melt pool data. By doing so, each frame monitored by the camera is categorized according to its position on the respective trajectory.
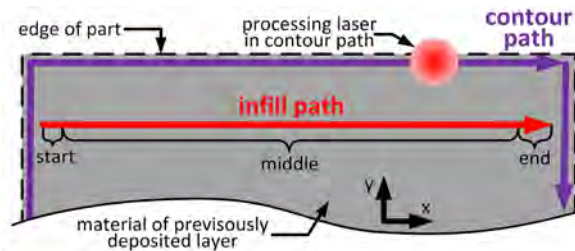
Fig. 5. Schematic draft of contour and infill path.

In this work, the following three categories with its specific subcategories are used:
- Infill path (subcategories: start, middle, end)
- Contour path (subcategories: start, middle, end)
- Laser-off

Examples of the camera images from the different path categories are presented in Fig. 6, which shows melt pool frames obtained within infill paths, contour paths and laser-off paths. All frames of infill paths are gathered during one trajectory, moving in the x direction, as the sketch in Fig. 5 shows. The Fig. shows camera frames at the start, middle and end of the infill path. The frames at the start of the infill path (time: 0 s to 0.11 s) show that the melt pool size gradually increases after the laser is switched on. In the camera images of the infill path, a typical oval shape of the melt pool is visible. The images show a higher intensity in the front of the melt pool compared to the rear. This fact is also confirmed in the investigations of other researchers (Turichin et al. 2022; Kledwig et al. 2019). One of the important factors responsible for such a non-uniform temperature distribution is the addition of the metal powder, which cools down. At the end of the infill path, the melt pool size decreases as the laser spot reaches an edge, and consequently, only a fraction of the laser

energy reaches the layer surface. While the laser is switched off, the intensity of heat radiation from the part surface drops, and no melt pool can be seen.

The images in the contour paths (Fig. 6), schematically shown in Fig. 5, are gathered in a segment, where only in the lower part of every frame the laser spot hits partially the sample surface. As the images show, the high heat radiation intensity is emitted predominantly in the lower part of the images. The melt pool in contour paths is therefore generally not as concentric to the laser beam as it is in infill paths.
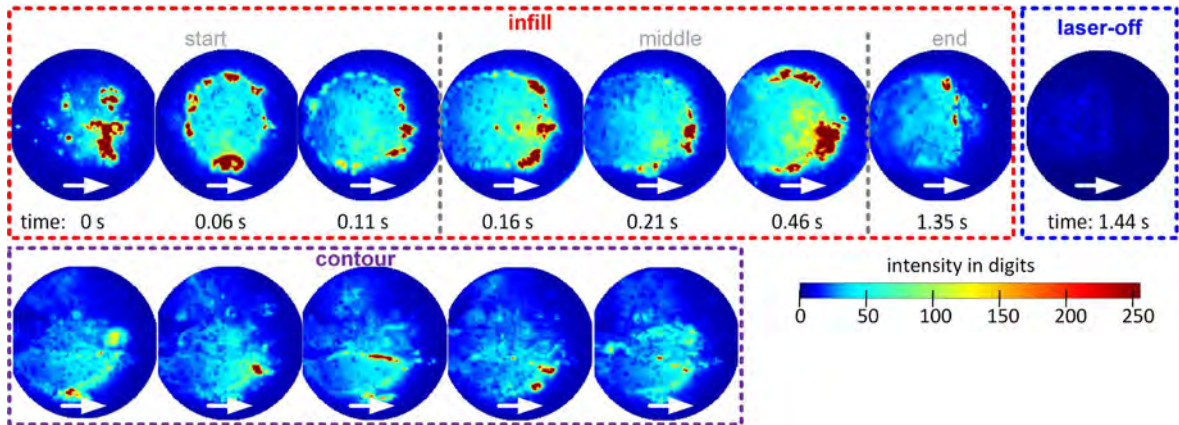
Fig. 6. Exemplary depiction of camera images gathered during respective processing conditions.

3.2. Temporal variation of melt pool characteristics

At first, the temporal progression of the melt pool size of one layer is discussed. Fig. 7 shows the progression of the detected melt pool size in the tenth layer of the built-up sample described above (Fig. 2). During laser-off paths, the detected melt pool size drops to zero. Laser-off paths are therefore excluded. A larger melt pool size is detected during the infill sequence compared to the contour sequence. This is due to the reduced overlap between the laser beam cross section and the part's upper surface and thus a reduced power input in the contour path. As explained, in each infill path, the melt pool size during the start and end sections is smaller relative to the one in the middle section. This is shown in more detail by one selected infill path in the lower segment of Fig. 7. The melt pool images at the three marked points in time are shown as well. As the time variation of the melt pool size is relatively small in the middle of the infill paths, the start and end sections of every path in the following analysis are excluded.
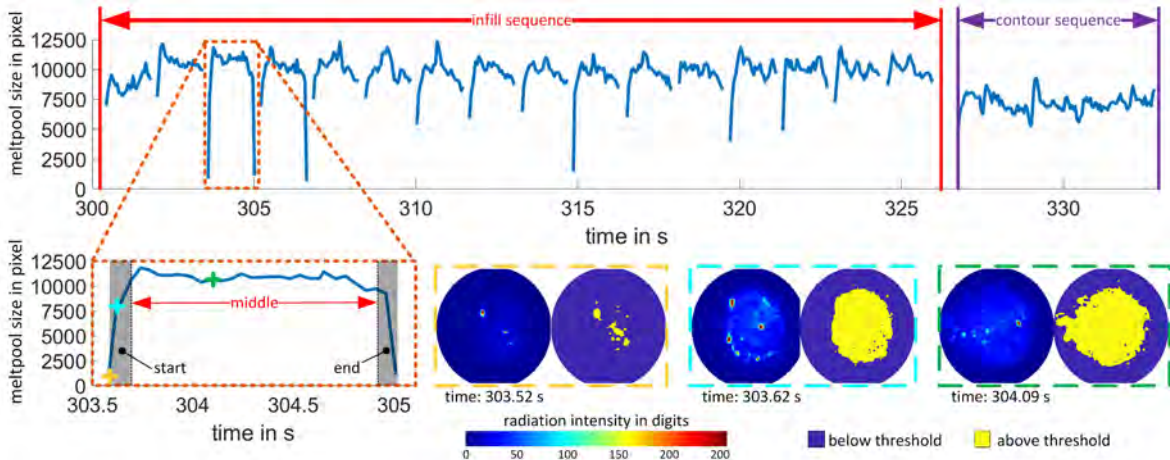
Fig. 7. Exemplarily depiction of temporal progression of melt pool size in infill and contour sequence of 10th layer.

Summarising the analysis of the melt pool variation within one layer, it can be concluded that disregarding laser-off segments as well as the start and end parts of infill and contour paths for further investigations is appropriate. In addition, the melt pool size in infill and contour trajectories should be considered separately from each other.

The temporal progression of the detected melt pool size during the entire building process is shown in Fig. 8 as lines. Infill sequences are shown as black lines. Contour sequences are shown as orange lines. The laser power in the respective layer is depicted by blue bars. The laser power is gradually reduced within the first eleven layers. Within these layers, the detected melt pool size shows a decreasing tendency as well. For layers beyond the eleventh layer, the process parameters remain unchanged. As can be seen, the temporal progression of the melt pool size shows an increasing tendency. This can be explained by the gradually increasing temperature of the sample due to heat accumulation.
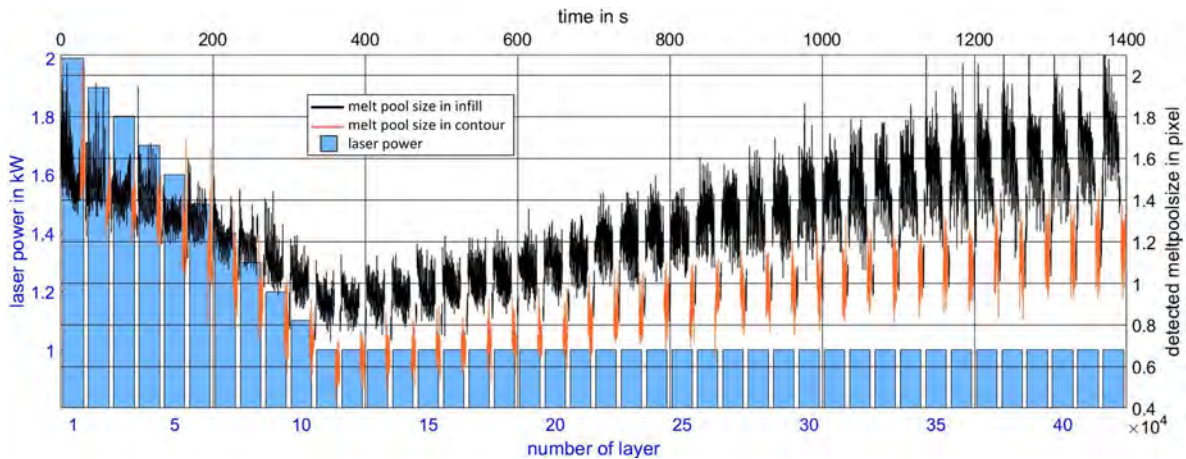
Fig. 8. Laser power in respective layer and temporal progression of melt pool size.

4. Detection and analysis of defects in samples

As mentioned above, the metallographic preparation and analysis of the built-up blocks for the detection of internal defects are applied. Fig. 9 shows the microscopy image of the cross section of a sample built-up with the process parameters described in Section 2.1. As the figure shows, local defects are present. The defects are predominantly present at the locations, where two adjacent weld beds are in contact with the underlying layer. These defects are typical lack of fusion defects, as described in (Dass und Moridi 2019). These types of defects result from a too small melt pool, which is the consequence of too low laser energy per unit length for specific local conditions.
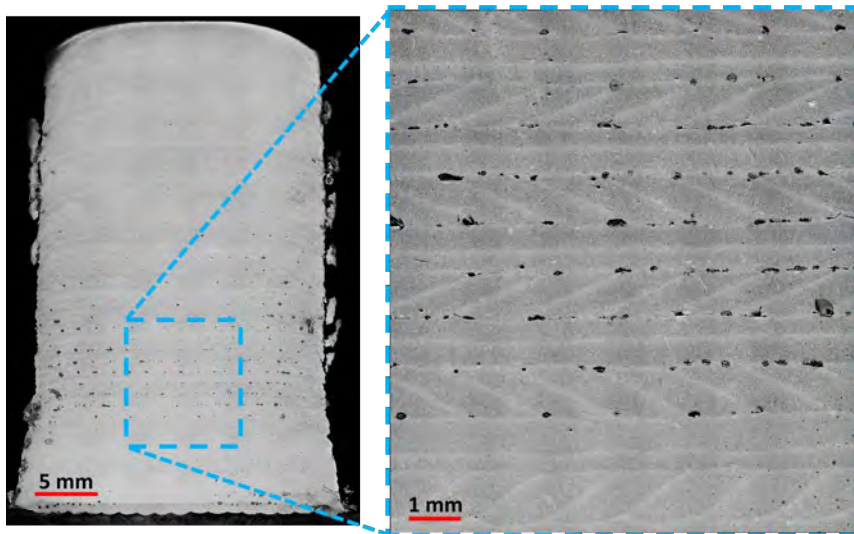
Fig. 9. Microscopy image of the cross section of one sample block.

The comparison of the melt pool size curve (Fig. 8) and the microscopy results leads to the conclusion that the location of the defects coincides with the locations of the detected reduced size of the melt pool. For the determination of the critical size of the melt pool below which the formation of the lack of fusion defects is possible, the process signals and the microscopy images can be compared. At the same time, the direct determination of the critical melt pool size using the curve from Fig. 8 is difficult. This time variation curve still exhibits large fluctuations in the melt pool signal.

To simplify the obtained signal, the following procedure incorporating the described categorization of the melt pool camera images can be used. As all paths within one layer use the same process parameters, the mean sizes of the melt pools can be calculated for all infill and contour paths within one layer. By that means, the process signals are further simplified. The mean size of the melt pools during infill trajectories is shown in Fig. 10 as grey bars. Contour trajectories are shown as light blue bars. As the figure shows, the locations at which lack of fusion defects are present coincide with the layers at which a mean infill melt pool size of less than approximately 12000 pixels is detected.

As the figure illustrates, in the first layer the mean melt pool size in infill and contour paths is practically comparable. This is because in both categories of trajectories, the whole cross section of the laser beam hits the substrate surface. With an increasing number of layers, the disparities between the mean values in infill and contour paths exhibit an increasing trend. This can be explained by the fraction of the laser beam energy that cannot reach a layer surface along contour paths. This stresses the need of categorizing of the acquired data concerning the trajectories.
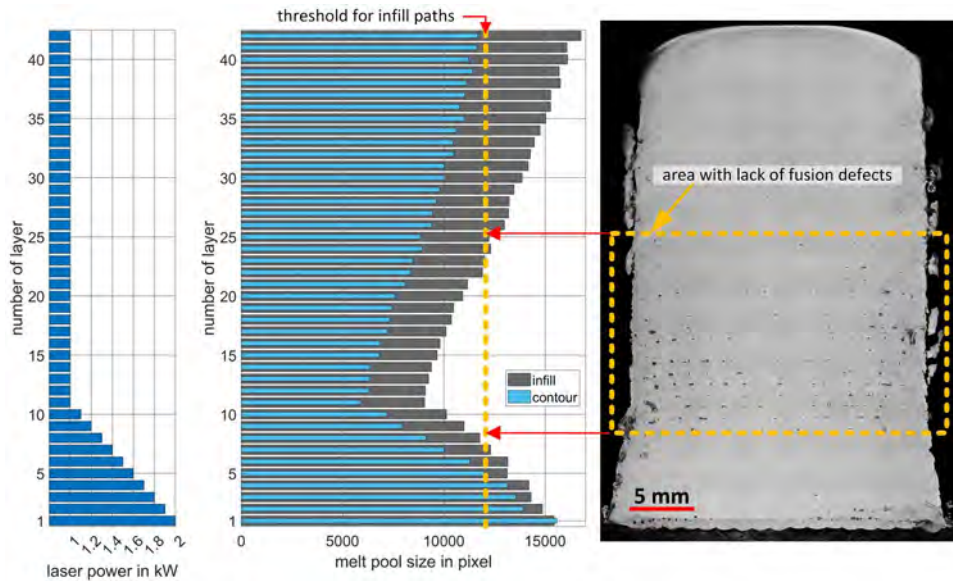
Fig. 10. Comparison of layer wise melt pool size during contour and infill paths with the distribution of defects in sample.

5. Conclusions

Monitoring of the melt pool by means of a coaxial camera enables the recording of melt pool characteristics during the LMD process. The melt pool size can be used as an important characteristic for evaluating the process stability and the final quality of built-up components. However, the radiation intensity signal, monitored by the camera, exhibits high fluctuations. Thus, a correlation between the monitored signal and the part's quality is complicated and has not been sufficiently investigated yet. Accordingly, process monitoring as well as the development of appropriate control strategies are difficult.

The analysis approach taken in this work is to interpret the recorded melt pool properties, accounting for the changing local conditions in the LMD process. Accordingly, a categorization of the recorded camera images is carried out for the different variants of trajectories. This way, it is considered whether frames are detected during infill, contour, or laser-off sequences. Furthermore, the averaging of the melt pool sizes in the infill and contour trajectories in the individual layers of a specimen is applied. The average melt pool size is shown to be sensitive to changes in laser power as well as temperature changes in the specimen. The potential of this metric to detect the formation of defects in the material has been investigated. The comparison of the monitoring data with metallographic examinations shows that in layers with observed lack of fusion defects, the average melt pool size in the infill paths falls below a certain threshold. It can be concluded that the average melt pool size in infill trajectories can be used as a parameter to assess the probability of the occurrence of the lack of fusion defects within the respective layer. To put this into practice, a calibration procedure for the determination of the lower limit for the melt pool size can be suggested. In addition to an improvement in process monitoring, this parameter has the potential to be implemented in an automated control of the process parameters.

Acknowledgements

References

Benarji, K.; Kumar, Y. Ravi; Paul, C. P.; Jinoop, A. N.; Bindra, K. S. (2020): Parametric investigation and characterization on SS316 built by laser-assisted directed energy deposition. In: Proceedings of the Institution of Mechanical Engineers, Part L: Journal of Materials: Design and Applications 234 (3), S. 452–466. DOI: 10.1177/1464420719894718.

Bennett, J.; Garcia, D.; Kendrick, M.; Hartman, T.; Hyatt, G.; Ehmann, K. et al. (2019): Repairing Automotive Dies With Directed Energy Deposition: Industrial Application and Life Cycle Analysis. In: J. Manuf. Sci. Eng 141 (2), 021019-1 bis 021019-9. DOI: 10.1115/1.4042078.

Bohlen, A.; Freiße, H.; Hunkel, M.; Vollertsen, F. (2018): Additive manufacturing of tool steel by laser metal deposition. In: Procedia CIRP 74, S. 192–195. DOI: 10.1016/j.procir.2018.08.092.

Dass, A.; Gabourel, A.; Pagan, D.; Moridi, A. (2022): Laser based directed energy deposition system for operando synchrotron x-ray experiments. In: Review of Scientific Instruments 93 (7), S. 75106. DOI: 10.1063/5.0081186.

Dass, A.; M., Atieh (2019): State of the Art in Directed Energy Deposition: From Additive Manufacturing to Materials Design. In: Coatings 9 (7), S. 418. DOI: 10.3390/coatings9070418.

Dey, N.: Additive manufacturing laser deposition of Ti-6Al-4V for aerospace repair application. MISSOURI UNIVERSITY OF SCIENCE AND TECHNOLOGY. Online verfügbar unter https://scholarsmine.mst.edu/masters_theses/7295.

Kersten, S.; Praniewicz, M.; Kurfess, T.; Saldana, C. (2020): Build Orientation Effects on Mechanical Properties of 316SS Components Produced by Directed Energy Deposition. In: Procedia Manufacturing 48 (3), S. 730–736. DOI: 10.1016/j.promfg.2020.05.106.

Khanzadeh, M.; Chowdhury, S.; Tschopp, Mark A.; Doude, Haley R.; Marufuzzaman, M.; Bian, L. (2019): In-situ monitoring of melt pool images for porosity prediction in directed energy deposition processes. In: IISE Transactions 51 (5), S. 437–455. DOI: 10.1080/24725854.2017.1417656.

Kledwig, C.; Perfahl, H.; Reisacher, M.; Brückner, F.; Bliedtner, J.; Leyens, C. (2019): Analysis of Melt Pool Characteristics and Process Parameters Using a Coaxial Monitoring System during Directed Energy Deposition in Additive Manufacturing. In: Materials (Basel, Switzerland) 12 (2). DOI: 10.3390/ma12020308.

Liu, Y.; Wang, L.; Brandt, M. (2019): Model predictive control of laser metal deposition. In: Int J Adv Manuf Technol 105 (1-4), S. 1055–1067. DOI: 10.1007/s00170-019-04279-9.

Ocylok, S.; Alexeev, E.; Mann, S.; Weisheit, A.; Wissenbach, K.; Kelbassa, I. (2014): Correlations of Melt Pool Geometry and Process Parameters During Laser Metal Deposition by Coaxial Process Monitoring. In: Physics Procedia 56, S. 228–238. DOI: 10.1016/j.phpro.2014.08.167.

Perini, M. (2020): Additive manufacturing for repairing: from damage identification and modeling to DLD processing.

Rey, P.; Prieto, C.; González, C.; Tzimanis, K.; Souflas, T.; Stavropoulos, P. et al. (2022): Data analysis to assess part quality in DED-LB/M based on in-situ process monitoring. In: Procedia CIRP 111, S. 345–350. DOI: 10.1016/j.procir.2022.08.036.

Schröcker, K.; Fichtl, M.; Bax, B.; Scheider, D.; Reisacher, M.; Prihodovsky, A. (2022): Mechanical properties of the LMD-processed material Ferro55 in as-built and heat-treated conditions. In: Procedia CIRP 111, S. 228–232. DOI: 10.1016/j.procir.2022.08.055.

Smoqi, Z.; Bevans, B. D.; Gaikwad, A.; Craig, J.; Abul-H., Alan; R., Brent et al. (2022): Closed-loop control of meltpool temperature in directed energy deposition. In: Materials & Design 215 (7), S. 110508. DOI: 10.1016/j.matdes.2022.110508.

Thompson, A.; Maskery, I.; Leach, R. K. (2016): X-ray computed tomography for additive manufacturing: a review. In: Meas. Sci. Technol. 27 (7), S. 72001. DOI: 10.1088/0957-0233/27/7/072001.

Turichin, G.; Mukin, D.; Valdaytseva, E.; Sannikov, M. (2022): Influence of Latent Heat of Fusion on the Melt Pool Shape and Size in the Direct Laser Deposition Process. In: Materials (Basel, Switzerland) 15 (23). DOI: 10.3390/ma15238349.

voestalpine Böhler Welding Group GmbH: Datasheet Ferro 55. Online verfügbar unter www.voestalpine.com/welding.

Wolff, S. J.; Wang, H.; Gould, B.; Parab, N.; Wu, Z.; Zhao, C. et al. (2021): In situ X-ray imaging of pore formation mechanisms and dynamics in laser powder-blown directed energy deposition additive manufacturing. In: International Journal of Machine Tools and Manufacture 166 (1), S. 103743. DOI: 10.1016/j.ijmachtools.2021.103743.